Mon. Not. R. Astron. Soc. **397,** 249–257 (2009) doi:10.1111/j.1365-2966.2009.14971.x

Quantifying the fast outflow in the luminous Seyfert galaxy PG1211+143

K. A. Pounds[1]★ and J. N. Reeves[2]

[1]*Department of Physics and Astronomy, University of Leicester, Leicester LE1 7RH*
[2]*Astrophysics Group, School of Physical and Geographical Sciences, Keele University, Keele, ST5 5BG*

Accepted 2009 April 24. Received 2009 April 23; in original form 2008 November 19

ABSTRACT

We report two new *XMM–Newton* observations of PG1211+143 in 2007 December, again finding evidence for the fast outflow of highly ionized gas first detected in 2001. Stacking the new spectra with those from two earlier *XMM–Newton* observations reveals strong and broad emission lines of Fe XXV and O VIII, indicating the fast outflow to be persistent and to have a large covering factor. This finding confirms a high mass rate for the ionized outflow in PG1211+143 and provides the first direct measurement of a wide angle, subrelativistic outflow from an active galactic nuclei (AGN) transporting mechanical energy with the potential to disrupt the growth of the host galaxy. We suggest PG1211+143 may be typical of an AGN in a rapid super-Eddington growth phase.

Key words: galaxies: active – galaxies: individual: PG1211+143 – quasars: general – galaxies: Seyfert – X-rays: galaxies.

1 INTRODUCTION

An early *XMM–Newton* observation of the bright quasi-stellar object PG1211+143 in 2001 provided strong evidence of a radial outflow of highly ionized gas with the remarkably high velocity of ∼0.13c (Pounds et al. 2003; Pounds & Page 2006). Unless viewed along the axis of a highly collimated flow, the high column density required to produce the observed Fe K absorption, combined with the high velocity, implied a mass outflow rate comparable to the accretion rate and transporting mechanical energy at a significant fraction of the bolometric luminosity. The broader potential importance of such energetic flows, which we have suggested might be typical of active galactic nuclei (AGN) accreting at the Eddington rate (King & Pounds 2003, hereafter K03), is in offering a feedback mechanism that could link the growth of supermassive black holes in AGN with their host galaxy (Ferrarese & Merritt 2000; Gebhardt et al. 2000; Tremaine et al. 2002; King 2003; Kim et al. 2008). The greatly improved sensitivity of current X-ray observations in the Fe K energy band is now yielding more examples of highly ionized outflows with large column densities and high velocities (see Cappi 2006 for a recent review), but the lack of information on the outflow collimation and covering factors (CFs) has left large uncertainties in the total mass and energy of these flows (Elvis 2006).

A second *XMM–Newton* observation, in 2004, found PG1211+143 to be in a brighter flux state, but with both the highly ionized and the moderately ionized spectral features responsible for the mid-band spectral curvature (and thereby contributing to a strong 'soft excess') significantly weaker. We now report two further *XMM–Newton* observations in 2007 December, finding the integrated X-ray flux to be higher again than in 2004. However, while the flux increase appears to be dominated by a soft continuum component, consistent with previous modelling of the broad-band X-ray spectrum of PG1211+143 (Pounds & Reeves 2007, hereafter P07), the blueshifted Fe K absorption is again clearly detected. We now combine data from all four observations of PG1211+143 in an attempt to characterize and quantify the re-emission from the highly ionized outflow and use this to clarify the flow structure, mass and energy.

We assume a redshift for PG1211+143 of $z = 0.0809$ (Marziani et al. 1996).

2 OBSERVATION AND DATA REDUCTION

The 2007 observations of PG1211+143 by *XMM–Newton* took place on December 21 and 23, with on-target exposures of ∼65 and ∼50 ks. In this paper, we use data from the EPIC pn and MOS cameras (Strüder et al. 2001; Turner et al. 2001) and the high-resolution reflection grating spectrometer (RGS; den Herder et al. 2001). Source counts from the EPIC cameras were taken from a circular region of ∼45 arcsec radius around the centroid position of PG1211+143, with simultaneous background spectra from a larger region, offset from but close to the target source. X-ray data were extracted with the *XMM* SAS v7.1 software and events selected corresponding to patterns 0–4 (single- and double-pixel events) for the pn camera and patterns 0–12 for the MOS cameras. Individual source spectra were integrated over the periods of low background and binned to a minimum of 20 counts per bin to facilitate use of χ^2 minimization in spectral fitting.

Spectral fitting was based on the XSPEC package (Arnaud 1996) and all fits included absorption due to the line-of-sight Galactic

★E-mail: kap@le.ac.uk

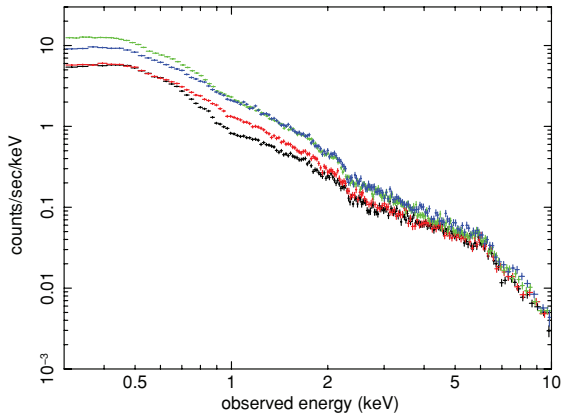

Figure 1. Comparison of the unmodelled pn spectra of PG1211+143 from the 2001 (black), 2004 (red), 2007a (green) and 2007b (blue) observations. As noted previously (P07), the differences between the 2001 and 2004 spectra can be largely attributed to weaker ionized absorption in 2004.

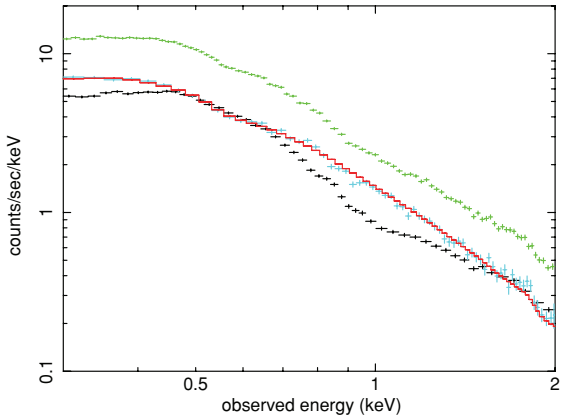

Figure 2. pn data from the 2001 (black) and 2007a (green) observations and the difference spectrum (light blue) obtained by a direct subtraction of the data sets. Modelling the difference spectrum finds a simple power law of $\Gamma \sim 3$ (red) to provide a good fit over the whole 0.3–10 keV EPIC band.

column of $N_{\rm H} = 2.85 \times 10^{20}\,{\rm cm}^{-2}$ (Murphy et al. 1996). Errors on individual parameters are quoted at the 90 per cent confidence level.

3 VISUAL EXAMINATION OF THE EPIC DATA

Fig. 1 displays the new pn spectral data of PG1211+143, together with data from the earlier *XMM–Newton* observations. In comparing such raw spectra, we note that each represents an integration of up to a day, with separations of 3, 6 years and 2–3 days. Visual examination of Fig. 1 suggests, however, that rather clear differences in such spectral 'snapshots' could be instructive in exploring spectral composition and variability. Thus, the ratio of the 2001 and 2004 EPIC count rate spectra (black and red in Fig. 1) led us to conclude (P07) that a decrease in continuum absorption was the main cause of the broad spectral change from 2001 to 2004. An important constraint on the nature of that variable absorption is the similarity in the ionizing flux during the 2001 and 2004 observations indicated by the near-identical spectra above ~3 keV, suggesting a change in CF rather than ionization parameter.

In both 2007 observations, PG1211+143 was a further factor of 2–3 brighter than in 2004, though again converging at the upper end of the EPIC energy band. In modelling the 2001 and 2004 spectra, we introduced a second continuum component which contributed strongly in the soft X-ray band (P07). Direct comparison of the highest (2007a) and lowest (2001) flux spectra now allows that model to be tested over a wider flux range. Fig. 2 shows the outcome, with the count rate difference spectrum being well fitted by a power law of $\Gamma \sim 3$, unaffected by continuum absorption.

We leave further discussion of this soft continuum component to another time while noting that – if a common property of luminous AGN – a soft, variable continuum substantially reduces the problem of the 'soft excess' widely debated over many years (e.g. Done et al. 2007 and references therein).

3.1 Further evidence for a high-velocity outflow

The most important outcome of the 2001 observation of PG1211+143 was the detection of blueshifted absorption lines of highly ionized Fe, S and Mg, initially interpreted (Pounds et al. 2003) as arising in highly ionized gas outflowing at ~0.1c. A more complete analysis of pn and MOS spectra, based on the detection of seven absorption lines of Ne, Mg, Si, S and Fe, removed an ambiguity on line identification, confirming a lower ionization parameter and correspondingly higher velocity of ~0.13c (Pounds & Page 2006). Emission lines were less well defined, and the model of P07 offered a possible explanation in terms of strong velocity broadening. The new observations in 2007 now provide the opportunity to test that proposal and further explore the properties of the ionized outflow in PG1211+143.

Fig. 3 shows the Fe K emission/absorption profiles from the 2001 pn data and the sum of the two 2007 observations. Each profile is the ratio of observed counts to an underlying continuum modelled by an absorbed power law over the 3–10 keV band. The data have been binned to minima of 50 and 100 counts, respectively, to improve the statistics in the highest energy channels. While the overall profiles in Fig. 3 are similar, with significant emission to the low-energy side of the ~7 keV absorption line in both data sets, the statistical quality of the individual profiles is clearly limited.

Obtaining a better-defined Fe K profile is important as the strength and width of an ionized emission component potentially carries crucial information on the CF and collimation of the outflow. That, in turn, is the key to determine the mass rate and mechanical energy in an outflow whose velocity is known. As we are interested in the time-averaged emission to assess the CF of the ionized outflow, and noting the essentially constant underlying continuum in the Fe K energy band (Fig. 1), it should be appropriate to utilize the integrated spectrum from all four *XMM–Newton* observations. In stacking the data from the different time periods, we used a weighted mean response function and adjusted the background scaling factor to account for the actual image areas used to collect individual data sets.

The Fe K profile from the stacked pn data is illustrated in Fig. 4 and resembles the P Cygni profile characteristic of an outflow, with both emission and blueshifted absorption components now better defined. While integrating the data from four observations, over 6 years, is likely to blur narrow or transient features, the improved statistics should offer a better measure of the average outflow properties.

We analyse the P Cygni profile in Section 5. Before that, the spectral model developed in P07 is refitted to the stacked data over the whole EPIC band in order to characterize the broad-band spectrum and possibly identify the spectral features that could contribute to the Fe K emission/absorption profile.

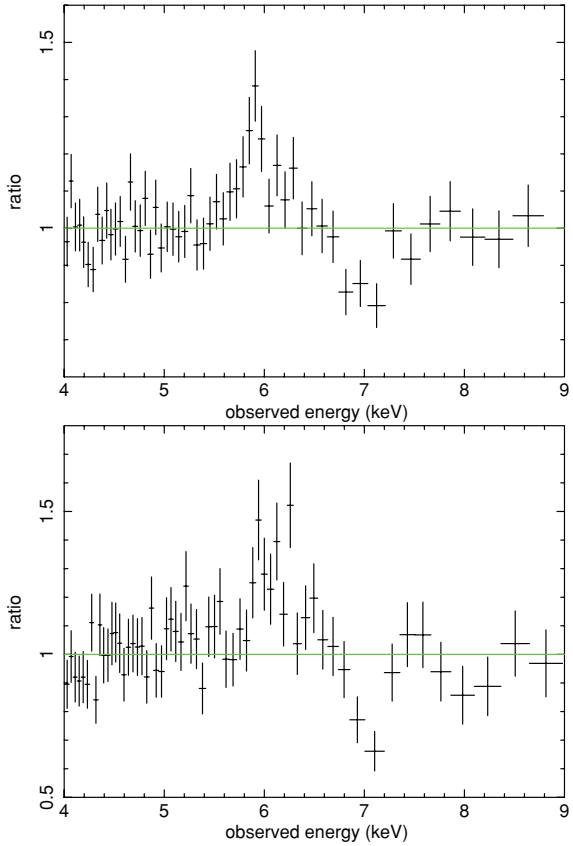

Figure 3. Fe K profiles expressed as a ratio of spectral data to a best-fitting continuum from the 2007 (top panel) and the 2001 (lower panel) pn observations of PG1211+143. While a narrow absorption line is seen near ∼7 keV in both profiles, the emission to lower energies is not well defined.

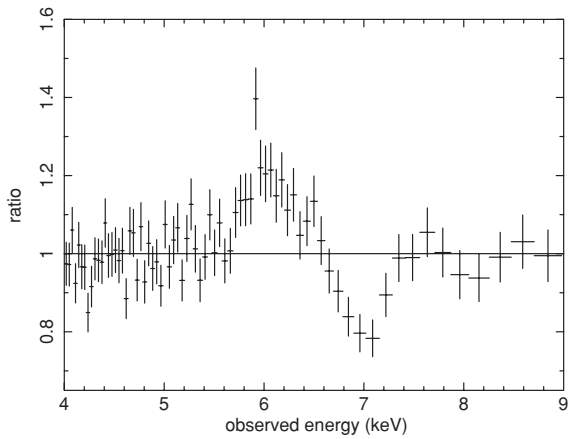

Figure 4. Fe K profile from the stacked pn observations of PG1211+143. The P Cygni like profile shows the emission and blueshifted absorption characteristic of an outflow are more clearly defined.

4 MODELLING THE OVERALL X-RAY SPECTRUM

The spectral model of P07 provided a physically consistent description of the broad-band X-ray spectra of PG1211+143 observed by *XMM–Newton* in 2001 and 2004. It has the form in XSPEC of wa(po1*abs1 + g1*em1 + g2*em2 + po2)abs2, with the 'primary' power-law (po1) modelling the energetically dominant continuum and a steeper continuum component (po2) found to dominate the soft X-ray variability. Photoionized absorption (abs1,2) and emission (em1,2) from highly and moderately ionized gas are modelled with the publicly available XSTAR grid 25, based on the revised treatment of Fe K (Kallman et al. 2004). Grid 25 has an assumed turbulence velocity of[1] 200 km s^{-1} and element abundances fixed at solar values (Grevesse & Sauval 1998). Free parameters in fitting the absorption and emission spectra are the ionization state, column density and apparent redshift, the latter being an indicator of the velocity of each photoionized gas component. Line broadening is allowed for in the model fit by convolving a separate Gaussian (g1, g2, modelled by GSMOOTH in XSPEC) with each emission line spectrum.

Applying this spectral model to the stacked pn and MOS data, separately, over the whole EPIC band yielded very similar fits, with the principal parameters listed in Table 1. The unfolded spectrum for the pn data is illustrated in Fig. 5.

The primary power-law component (po1) has a photon index of $\Gamma \sim 2$–2.1 and is strongly absorbed by moderately ionized gas of column density $N_{\rm H} \sim 8 \times 10^{22}$ cm^{-2} and ionization parameter $\log \xi \sim 2.0$ erg cm s^{-1}. The secondary power law (po2) has a much steeper slope ($\Gamma \sim 2.8$–2.9) and is affected only by the more highly ionized absorber.

The highly ionized absorber has a well-constrained ionization parameter in both pn and MOS fits, with $\log \xi \sim 3.4$ and a large column density $N_{\rm H} \sim 8 \times 10^{23}$ cm^{-2}. The 'apparent redshift' is ~ -0.026, implying the absorbing gas is strongly blueshifted in the rest frame of PG1211+143. As the redshift measure is dependent on the primary line identification (and hence ionization parameter) in the modelling, these important parameters are not independent. To explore this dependence, we obtained confidence contours for the ionization parameter and redshift of the highly ionized absorber component with all other model parameters free. Fig. 6 shows the outcome of this check, confirming an ionization parameter of $\log \xi \sim 3.37$ and apparent redshift of -0.025 ± 0.005. Converting apparent redshift to the rest frame of PG1211+143 gives an outflow velocity for the highly ionized gas of $\sim 0.099 \pm 0.005$c. The precision of this velocity measure, which derives from fitting to the strong Fe XXV line and an array of comoving absorption lines best seen in the 2001 data (Pounds & Page 2006), is probably misleading given the assumption of a unique ionization parameter for the fast outflow.

The model fit for the moderate ionization absorber yielded an apparent redshift of 0.02 ± 0.01 and a significantly lower outflow velocity of $\sim 0.06 \pm 0.01$c.[2]

The photoionized emission spectra were found to have ionization parameters of $\log \xi \sim 3.2$ and 1.2, both with apparent redshifts of 0.08 ± 0.01, indicating a low mean velocity relative to the AGN. Importantly, the coincidence of absorption and emission ionization parameters for the fast outflow implies these are from the same flow component. In contrast, significant re-emission from the moderately ionized gas was not required in the spectral fit, suggesting it has a small emission measure.

[1] A higher turbulent velocity would result in lower column densities but would not significantly alter the main results of this analysis

[2] For ionization parameters in the range $\log \xi \sim 1.8$–2.4, the XSTAR models predict inner-shell (1s-2p) absorption at ∼6.5 keV from Fe XVIII–XXIII (Behar & Netzer 2002). For an outflow velocity of ∼0.06c, this feature would be observed at ∼6.3 keV in PG1211+143. Intriguingly, Fig. 7 does show a small dip at 6.35 ± 0.05 keV, although this is only marginally significant in the present data.

Table 1. Parameters of the model fit to the stacked pn and MOS data from the 2001, 2004 and 2007 *XMM–Newton* observations of PG1211+143.

	Γ_1	Γ_2	N_H	log ξ	Redshift	N_H	log ξ	Redshift	χ^2/d.o.f.
pn	2.09 ± 0.09	2.92 ± 0.02	7.8	2.04 ± 0.02	0.022 ± 0.001	82	3.37 ± 0.01	-0.026 ± 0.004	548/478
MOS	2.03 ± 0.10	2.78 ± 0.04	7.7	2.03 ± 0.03	0.010 ± 0.001	90	3.36 ± 0.01	-0.024 ± 0.01	398/354

Note. Power-law indices Γ_1 and Γ_2 refer to the primary and secondary continuum components, respectively. High- and moderate-ionization absorbers affect the primary continuum, with equivalent hydrogen column densities in units of 10^{22} cm^{-2} and ionization parameters in erg cm s^{-1}. The soft secondary continuum is affected only by the high-ionization absorber. Apparent redshifts are converted to ionized gas outflow velocities in the text.

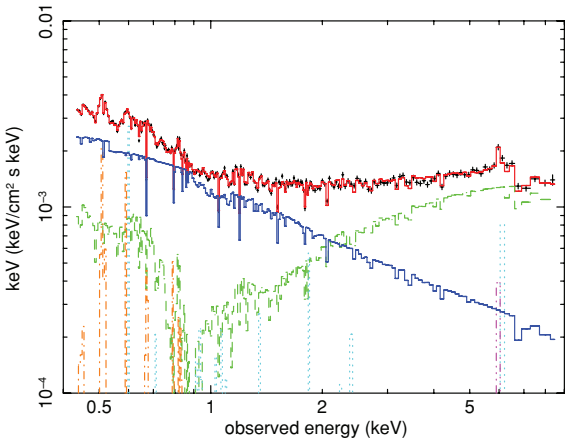

Figure 5. Unfolded broad-band model fitted to the stacked pn spectral data. The continuum components are shown in green and dark blue, and the ionized gas emission spectra in light blue and brown. A narrow emission line (pink) has been added to represent the feature found in the Gaussian fitting described in the next section and attributed to Fe Kα fluorescence from cold matter.

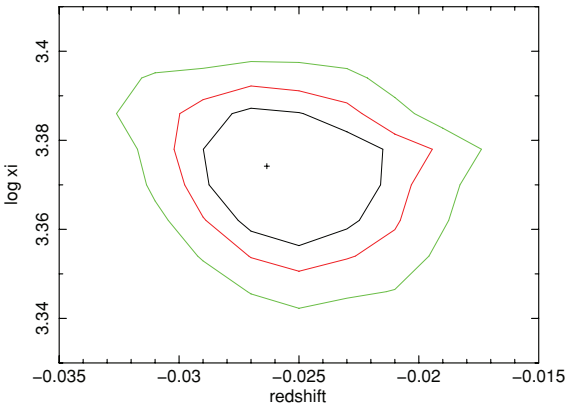

Figure 6. 68, 90 and 99 per cent confidence contours for the ionization parameter and apparent redshift of the highly ionized component of the outflow, assessed with all model parameters free in the pn data fit.

Importantly, strong broadening of the high-ionization emission lines is implied by the parameter g1, for which a value $\sigma \sim 340 \pm 180$ eV at 6 keV (with constant $\Delta E/E$) significantly improved the quality of the fit [reducing χ^2 by 17 for one fewer degrees of freedom (d.o.f.)], while allowing the line fluxes to increase by a factor of ~5. In contrast, the Gaussian broadening parameter for the low ionization gas, $\sigma \sim 60$ eV, was found to make very little difference to the overall spectral fit.

Visual examination of Fig. 5 suggests that only the highly ionized gas (light blue in the figure) is likely to contribute significant line emission in the Fe K band, with a strong resonance line of He-like Fe XXV (rest energy 6.7 keV). Blueshifted Fe XXV is also identified with the strongest absorption line arising from the highly ionized gas, while the lower ionization column results in a significant Fe K absorption edge and curvature in the primary (po1) continuum.

It is particularly interesting that the spectral fit requires the highly ionized emission line spectrum to be strongly broadened. Deconvolution of the Fe K profile in the stacked data offers the promise of a direct measure of this broadening in the case of a dominant Fe XXV emission line, thereby providing a key indicator of the geometry of the outflow.

5 RESOLVING THE P Cygni PROFILE OF Fe K IN THE EPIC DATA

Fig. 4 shows the profile of Fe K emission and absorption for the stacked pn data, plotted as a ratio to the best-fitting continuum. Guided by the broad-band model fitted in the previous section, the continuum is modelled over the 3–10 keV band with the form in XSPEC wa(zwa*po1 + po2), where zwa allows for absorption of the primary power law at the redshift of PG1211+143. A best-fitting continuum was found for power-law indices of $\Gamma = 2.2$ and 2.9, with a cold absorbing column of 10^{23} cm^{-2}. Tests showed these parameters are important in determining the details of the P Cygni profile deconvolution, mainly in the deduced line strengths, but do not change the need for two dominant components, one in absorption at ~7 keV and a broader emission component at a lower energy.

We initially analysed the P Cygni line profile by adding a sequence of positive and negative Gaussians to produce a visual and quantitative fit. The main profile was found to be well fitted by the addition of just two lines, both broader than the resolution of the pn camera. Fig. 7 shows this fit, with emission and absorption component energies (adjusted to the redshift of PG1211+143) of 6.51 ± 0.04 and 7.65 ± 0.05 keV, and 1σ linewidths (which here include ~65 eV for the pn resolution) of 210 ± 50 and 170 ± 50 eV, respectively. The statistical improvement by adding these two Gaussians is listed, together with the individual component parameters, in Table 2.

Although already a good fit, the emission component in Fig. 7 has an obvious high data point which lies close to 5.92 keV, which corresponds (at the redshift of PG1211+143) to the 6.4 keV Fe Kα line, often seen in the spectra of AGN and attributed to fluorescence from low-velocity (distant?) cold matter. Adding a third Gaussian to the profile fit, with width constrained to the pn energy resolution, gave a further small but significant improvement to the fit, while increasing the energy of the broad emission component to 6.61 ± 0.08 keV and its width to 260 ± 60 eV. The absorption line parameters were essentially unchanged. Fig. 8 reproduces this three-Gaussian fit with parameters summarized in Table 2.

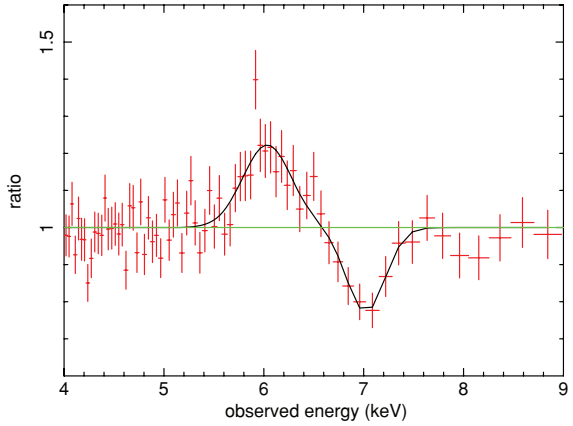

Figure 7. Double Gaussian line fit to the stacked pn data Fe K profile showing a classical P Cygni profile.

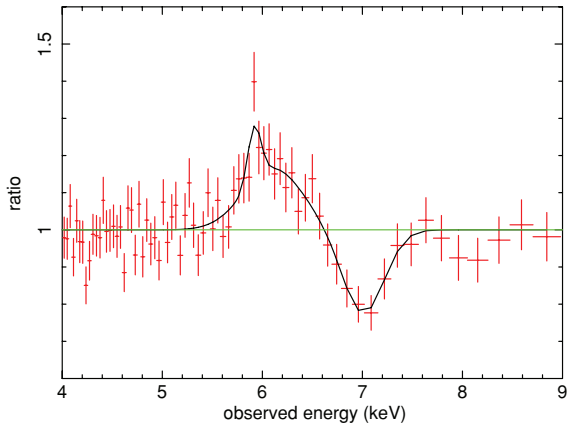

Figure 8. Fig. 7 with an additional narrow emission line at the rest energy of Fe Kα.

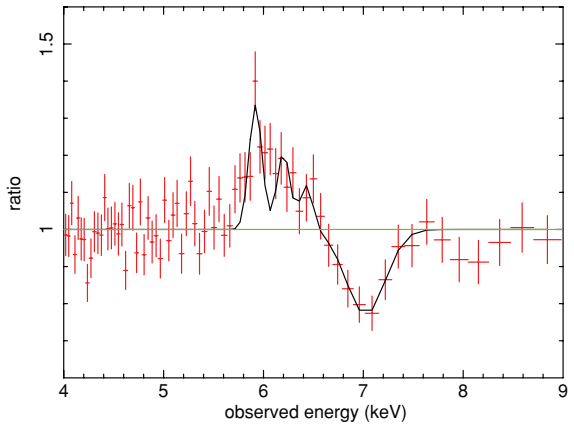

Figure 9. An alternative Gaussian fit to the Fe K profile with a narrow emission line corresponding to neutral Fe Kα (rest energy 6.4 keV) and resonance emission lines of Fe XXV (6.7 keV) and Fe XXVI (6.97 keV).

The broad emission component is now consistent with the resonance 1s-2p transition in He-like Fe XXV, the same transition as identified in the absorption spectrum in the 2001 data (Pounds & Page 2006). Allowing for the pn camera resolution, an intrinsic emission linewidth of 250 ± 60 eV, or 28 000 ± 7000 km s^{-1} [full width at half-maximum (FWHM)] when interpreted solely in terms of velocity broadening, corresponds to a wide-angle outflow of semi-angle $\sim 50^{\circ}$. With the reasonable assumption that the Fe XXV emission and absorption lines come from the same ionized outflow, the comparable equivalent widths (EWs) of the two components is further strong evidence for the outflow having a large CF.

The significantly narrower absorption line in the stacked data constrains the effects of velocity variations and (unknown) turbulence, while also ruling out a significant change in the ionization state of the highly ionized gas, for example from dominantly Fe XXV to Fe XXVI. We conclude that the greater broadening of the emission line with respect to the absorption line in the stacked data is most likely due to the spread of projected velocities in a wide-angle flow.

To check the robustness of the broad ionized emission line in the stacked data, an alternative fit was tried with three narrow emission lines corresponding to neutral Fe Kα (rest energy 6.4 keV) and the resonance emission lines of Fe XXV (6.7 keV) and Fe XXVI (6.97 keV). The fit was notably worse ($\Delta\chi^2 = 38$) than that with the narrow Fe Kα plus broad Fe XXV emission line (Fig. 9).

Finally, to confirm the broad emission line is not an artefact of the stacking procedure the four pn data sets (Fig. A1 in Appendix A) were fitted individually. Although less well determined, a broad Fe K emission line is preferred in each individual data set, with widths and line energies consistent, within the errors, with those derived for the stacked data (Appendix A, Table A1).

In summary, analysis of the Fe K line profile provides evidence for a velocity-broadened emission line at a rest energy consistent with the principal resonance transition of Fe XXV. As Fe XXV is also identified as the ionization state in the highly ionized absorber, it is reasonable to interpret the emission component in the P Cygni profile with the same outflow. We note that this conclusion, including the emission line broadening, is also consistent with the description of the broad-band X-ray spectrum of PG1211+143 in Section 4.

6 A CHECK FOR CONSISTENCY IN THE RGS SPECTRUM

The unfolded spectrum in Fig. 5 suggests that discrete spectral features might also be visible in the soft X-ray band. If so, the higher resolution of the *XMM–Newton* RGS could provide a further constraint on the broadening of emission lines from the highly

Table 2. Parameters of Gaussian absorption and emission lines sequentially fitted to the ratio of stacked pn data to continuum over the 3–9 keV band.

Fit	Energy	Width	EW	Energy	Width	EW	Energy	Width	EW	$\Delta\chi^2$ d.o.f.
1	7.60 ± 0.05	0.19 ± 0.06	−120 ± 30							49/3
2	7.65 ± 0.05	0.17 ± 0.05	−110 ± 40	6.51 ± 0.04	0.21 ± 0.05	150 ± 45				47/3
3	7.65 ± 0.05	0.16 ± 0.06	−110 ± 45	6.61 ± 0.08	0.26 ± 0.06	135 ± 45	6.4	65	25 ± 10	5/1

Note. Line energies (adjusted to the AGN redshift) and 1σ linewidths are in keV and EWs in eV. The final column gives the improvement in χ^2 for each successive fit.

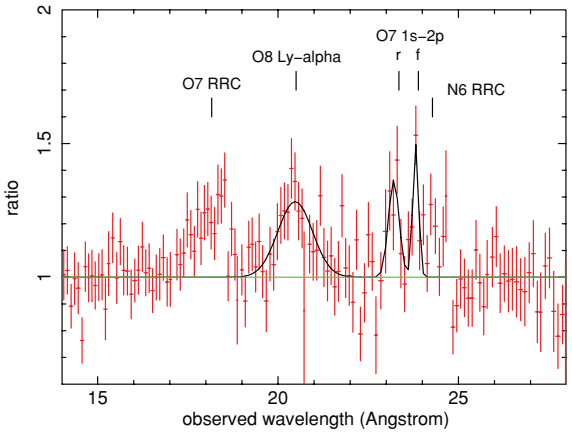

Figure 10. Gaussian fits to the stacked RGS data show a broad emission line of O VIII Lyman-α and a less broad O VII 1s-2p resonance line. Also shown is a narrow emission line identified with the forbidden transition in O VII and RRC of O VII and N VI. The rest wavelengths of the identified features are indicated.

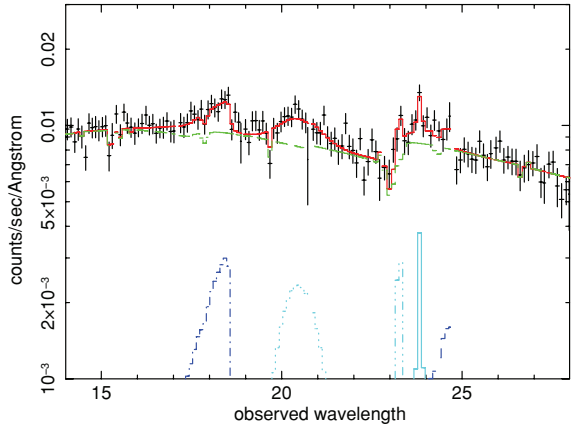

Figure 11. The stacked RGS data compared with a power law of $\Gamma \sim 2.9$ (green) together with the spectral features (blue) detailed in Table 3.

ionized outflow, as H-like ions of O and Ne will co-exist with He-like Fe XXV.

To check this possibility, the spectra from all four RGS observations were stacked in the same way as for the EPIC data, and the ratio of the background-subtracted data to a best-fitting power law (we found $\Gamma \sim 2.9$, in agreement with the po2 component in Table 1) over the 14–28 Å band was derived. The data were then regrouped in nine-channel bins to reduce random noise, giving an effective spectral resolution of ~0.1 Å.

Fig. 10 shows the resulting RGS data:continuum spectral ratio and marks the rest wavelengths of the principal emission lines of O VII and O VIII, together with the edge energies of the recombination continua of O VII and N VI. As with the Fe K line profile, Gaussians were fitted to the three most obvious emission lines, with wavelength, width and amplitude as free parameters.

Of particular interest is a well-defined – and strong – O VIII Lyman-α line, as predicted in Fig. 5. The Gaussian fitting finds a wavelength of 20.48 ± 0.08 Å (18.95 ± 0.08 Å at the redshift of PG1211+143), with a linewidth of $\sigma = 0.42 \pm 0.08$ Å. Interpreted in terms of velocity broadening, the linewidth corresponds to ~14 000 ± 5500 km s^{-1} (FWHM). While significantly lower than the value found from fitting the Fe XXV emission line in the EPIC data, the higher intrinsic resolution of the RGS does hint at a narrower core and broader wings than modelled by the simple Gaussian line.

The O VII (1s-2p) resonance line is also clearly detected in the stacked RGS data, at 23.22 ± 0.06 Å (21.48 ± 0.05 Å), but is significantly less wide than the higher ionization O VIII line, with $\sigma = 0.16 \pm 0.05$ Å. Again, this result is consistent with the narrower Gaussian smoothing factor required for emission from the less ionized gas in the model of Fig. 5. Also seen in Fig. 10 is an unresolved line very close to the rest wavelength of the forbidden line in the O VII 1s-2p triplet. We surmise that this emission arises from a low-density component of the outflow, presumably at a substantially larger radial distance than the velocity-broadened lines.

Two other spectral features in Fig. 10 are identified with radiative recombination continua (RRC) of O VII and N VI. Fitting a more appropriate delta function in XSPEC yields an electron temperature of ~ 0.03 ± 0.01 keV for the stronger O VII RRC.

Table 3 lists the parameters of all five spectral features identified in the stacked RGS data, giving an overall improvement to the power-law fit of $\Delta\chi^2 = 102$ for 15 additional d.o.f. Fig. 11 shows the contribution of the five components to the overall spectrum.

In summary, the stacked RGS data confirm significant photoionized emission in the soft X-ray spectrum of PG1211+143 as indicated in the spectral model of Fig. 5, and provide further support (particularly from the strength and broadening of the O VIII Lyman-α line) for the large CF of the highly ionized outflow implied by the strong and broad Fe XXV resonance emission in the EPIC data.

7 DISCUSSION

7.1 A persistent high-velocity outflow

A significant, but variable strength absorption line has now been observed at ~7 keV in three of the four *XMM–Newton* observations of PG1211+143, and also in an observation from Suzaku (Reeves et al. 2008). The most recent *XMM–Newton* observations, reported

Table 3. Parameters of the principal emission features in the stacked RGS data.

Feature	Obs. wavelength	Lab wavelength	1σ linewidth	RRC kT (eV)	EW (eV)	$\Delta\chi^2$/ d.o.f.
O VII RRC	17.2 ± 0.1	16.80		30 ± 9	12.6 ± 3.5	38/3
O VIII Lyman-α	18.95 ± 0.1	18.97	14 000 ± 3000		11.8 ± 3.8	36/3
O VII 1s-2p (r)	21.5 ± 0.1	21.60	5000 ± 1600		2.4 ± 1.1	11/3
O VII 1s-2p (f)	22.05 ± 0.05	22.1	1500 ± 900		1.7 ± 1.0	10/3
N VI RRC	22.45 ± 0.15	22.46		15 ± 10	3.7 ± 2.0	7/3

Note. The emission line and RRC edge wavelengths (adjusted to the AGN redshift) are in Angstrom with 1σ linewidths in km s^{-1} (FWHM).

here, show the subrelativistic, highly ionized outflow, originally discovered in the 2001 *XMM–Newton* observation, to be persisting.

Identifying the ∼7 keV absorption line with Fe XXV, as in the initial 2001 spectrum (Pounds & Page 2006), is consistent with the ionization parameter derived from modelling the broad-band stacked data. That model, outlined in Section 4, finds a mean velocity for the highly ionized outflow of ∼0.10c, from both pn and MOS fits. Gaussian fitting to the Fe K profile in Section 5 finds a slightly higher absorption line energy, and implied outflow velocity of ∼0.12c. In the following discussion, we assume a mean outflow velocity for the stacked data of 0.11c.

Evidence for actual variability in the outflow velocity is offered by the absorption component being broader in the stacked data than in the initial observation of 2001. On that interpretation, the measured width of $\sigma = 160 \pm 60$ eV, or 145 ± 60 eV allowing for the pn resolution, corresponds to a velocity spread of ±0.02c.

The persistence of the blueshifted absorption over a 6 years period suggests, unless the flow is highly collimated or recombination times very short, that we should expect to find evidence for an extended region of re-emission integrated over the outflow. Detecting broad and strong emission lines of Fe XXV and O VIII from the same highly ionized gas now provides confirmation of that expectation and provides the key information lacking in previous observations of high-velocity outflows, namely the CF. In turn, the CF allows the actual mass and energy in the flow to be quantified.

7.2 An energetically important outflow

We now combine the fitted parameters for the stacked data from Sections 4–6 to re-assess the structure and hence the wider significance of the fast outflow in PG1211+143.

We have three ways of assessing the flow geometry or CF of the highly ionized gas. The most direct is to compare the strength of the Fe XXV absorption and emission components in the P Cygni profile. The similar EWs of the main absorption and emission components in the Fe K profile deconvolution in Section 5 indicates a CF ∼ 1 if the emission is simply from resonance line absorption and re-emission (scattering). While this estimate is subject to some uncertainty due to the different time-scales of the absorption and emission measures, and to the density dependance of an additional recombination emission component, a highly collimated flow is strongly ruled out, with a conservative CF ∼ 0.5.

A second estimate of the CF can be obtained, as in P07, by comparing the total continuum energy absorbed and re-emitted by the highly ionized gas components in modelling the stacked broad-band EPIC data. For the pn data, we find the luminosity of the highly ionized line emission spectrum to be 4.3×10^{42} erg s^{-1} while the energy absorbed from the continuum by the highly ionized gas is $\sim 1.3 \times 10^{43}$ erg s^{-1}, yielding a CF ∼ 0.33. The corresponding quantities in the MOS spectral fit are 9.8×10^{42} and 1.7×10^{43} erg s^{-1} giving a CF ∼ 0.57. While these estimates are derived from a rather complex model, we believe they are reliable to a factor of 2.

The third signature of flow geometry is from the observed emission linewidths. In that respect, it is significant that an acceptable fit to the broad-band EPIC data required the highly ionized emission lines to be broad. Only by including the Gaussian broadening parameter in the spectral fitting was the emission line spectrum allowed to increase in strength to match the spectral structure in the data. For the pn data in Section 4, we found a Gaussian width of $\sigma \sim 340 \pm 180$ eV (at 6 keV), consistent with the value $\sigma \sim 250 \pm 60$ eV derived from the line profile fitting in Section 5. [We recall the emission line component in the Fe K profile in a 2005 Suzaku observation of PG1211+143 appears very similar to that in the stacked *XMM–Newton* data, with a mean energy of ∼6.5 keV and width of $\sigma \sim 250$ eV (Reeves et al. 2008).] Assuming a Gaussian width of $\sigma \sim 250 \pm 60$ eV and the assumption of velocity broadening in a radial flow then correspond to a flow cone of half angle ∼50° and CF ∼ 0.3.

Importantly, all the above indicators show the highly ionized outflow is *not* highly collimated, and therefore involves a significant mass loss. The mass outflow rate in a uniform radial outflow of velocity v is given by $\dot{M}_{\rm out} = 4\pi b n r^2 m_{\rm p} v$, where b is the covering fraction, n is the gas density at a radial distance r and $m_{\rm p}$ is the proton mass. We obtain nr^2 $(=L_{\rm ion}/\xi)$ from the broad-band model of Section 4 which has a relevant ionizing X-ray luminosity $L(\geq 7$ keV) of 2×10^{43} erg s^{-1} and an ionization parameter $\xi(=L/nr^2) \sim 2350$, yielding $nr^2 \sim 8.5 \times 10^{39}$ cm^{-1}. For a mean velocity of 0.11c, the mass-loss rate is then $\dot{M}_{\rm out} = \sim 5.8b \times 10^{26}$ gm s^{-1}($\sim 8.7b$ M$_\odot$ yr^{-1}).

Assuming from the above estimates a value of $b = 0.4$, we find an average outflow mass rate over the four *XMM–Newton* observations of $\dot{M}_{\rm out} \sim 3.4$ M$_\odot$ yr^{-1}. This compares with $\dot{M}_{\rm Edd} = 1.6$ M$_\odot$ yr^{-1} for a non-rotating supermassive black hole of mass $\sim 4 \times 10^7$ M$_\odot$ (Kaspi et al. 2000) accreting at an efficiency of 10 per cent. The average mechanical energy in the fast outflow is then of the order of $\sim 1.3 \times 10^{45}$ erg s^{-1}.

7.3 A continuum driven outflow from a super-Eddington AGN

K03 described a simple model in which black holes accreting at or above the Eddington rate can drive winds which are, at small radii, Compton thick in the continuum. It seems likely that this mechanism is responsible for the highly ionized outflow in PG1211+143, as the line driving favoured to explain outflows in Broad Absorption Line galaxies is ruled out for such highly ionized gas.

The assumption in K03 is that the matter decouples from the photons at the boundary of the Compton thick flow (the photosphere) and is launched with an outflow velocity equal to the escape velocity at that radius $R_{\rm launch}$. Here, we have $v \sim 0.11$c, which corresponds to $R_{\rm launch} \sim 80 R_{\rm s}$ (where $R_{\rm s} = 2GM/c^2$ is the Schwarzschild radius), or 5×10^{14} cm for PG1211+143. The EPIC data show significant flux variability on time-scales of 2–3 h (fig. 1 in Pounds et al. 2003), which would be compatible with the above scale size relating to the primary (disc/corona) X-ray emission region.

An important prediction of the black hole winds model of K03 is that the outflow momentum will be simply related to the Eddington luminosity, viz $\dot{M}_{\rm out} v = L_{\rm Edd}/c$, an equivalence that can be tested for PG1211+143. Using the mass rate and velocity for the stacked data, we have $\dot{M}_{\rm out} v = 2.5 \times 10^{35}$ and, for an AGN mass of 4×10^7 M$_\odot$ (Kaspi et al. 2000), $L_{\rm Edd}/c = 1.7 \times 10^{35}$ – in reasonably good agreement with the continuum driving model.

The location and structure of the lower ionization absorber, responsible for most of the continuum absorption in our model, are unclear. The lower velocity indicated by our spectral fitting suggests a separate flow component. With an imprint only on the primary continuum, it seems that this $\log \xi \sim 2$ matter exists close to the inner accretion disc, while the absence of substantial line emission from that matter implies a small emission measure, possibly constrained in small, higher density clouds (e.g. Risaliti et al. 2005). That possibility could be tested for PG1211+143 by more extended observations to constrain the time-scale on which the primary continuum absorption is seen to change.

In an extension of the model of K03, a possible scenario might be where an inhomogeneous flow accretes through the inner disc to a radius R where radiation pressure causes the matter to be launched at the local escape velocity. As the outflow expands outwards, the mean density will fall, as will the filling factor of the cooler, more opaque, matter.

In conclusion, we suggest that the unusual properties of PG1211+143 (at least among local AGN) are due to a super-Eddington accretion rate, a condition expected to apply to galaxies in their rapid growth phase. In that sense, PG1211+143 might be described as a late developer. However, we note that if the current outflow rate is maintained for 2×10^7 years, the mechanical energy of $\sim 10^{60}$ erg carried into the host galaxy would exceed the binding energy for a typical Galactic bulge containing 10^{11} stars with a velocity dispersion of 300 km s^{-1}.

8 SUMMARY

(1) New *XMM–Newton* observations of PG1211+143 in 2007 have found the subrelativistic outflow of highly ionized gas first seen in 2001 to be persisting.

(2) Stacking all existing EPIC data has shown a classical P Cygni line profile to describe the emission and absorption components in the Fe K band. Deconvolving those components finds a broad emission line close to the rest energy of the resonance line of Fe XXV, the principal ionization state previously identified in the high-velocity absorption spectrum.

(3) Interpreting the emission linewidth in terms of velocity broadening indicates the fast outflow is occurring over a wide cone, while the large EW of the Fe XXV emission line is further direct evidence of a strong and persistent outflow of highly ionized gas.

(4) Refitting the broad-band spectral model of P07 to the stacked data allows the time-averaged absorption and re-emission by the high-ionization gas to be quantified, yielding a separate estimate of the CF of the fast outflow, of ~0.3–0.6.

(5) These X-ray data provide the clearest evidence to date of an AGN outflow carrying sufficient mechanical energy to disrupt starburst growth and provide the predicted coupling of the growth of a supermassive black hole and the host galaxy.

(6) We suggest that PG1211+143 is a rare example of a bright, low-redshift, type 1 AGN accreting at the Eddington limit.

ACKNOWLEDGMENTS

The results reported here are based on observations obtained with *XMM–Newton*, an ESA science mission with instruments and contributions directly funded by ESA Member States and the USA (NASA). The authors wish to thank Valentina Braito for re-extracting the earlier PG1211+143 spectra and the SOC and SSC teams for organizing the *XMM–Newton* observations and initial data reduction.

REFERENCES

Arnaud K. A., 1996, in Jacoby G. H., Barnes I., eds, ASP Conf. Ser. Vol. 101, Astronomical Data Analysis Software. Astron. Soc. Pac., San Francisco, p. 17
Behar E., Netzer H., 2002, ApJ, 570, 165
Cappi M., 2006, Astron. Nachr., 327, 1012
den Herder J. et al., 2001, A&A, 365, L7
Done C., Sobolewska M. A., Gierlinski M., Schurch N. J., 2007, MNRAS, 374, L15
Elvis M., 2006, Mem. della Soc. Astron. Ital., 77, 573
Ferrarese L., Merritt D., 2000, ApJ, 539, L9
Gebhardt K. et al., 2000, ApJ, 539, L13
Grevesse N., Sauval A. J., 1998, Space Sci. Rev., 85, 161
Kallman T., Palmeri P., Bautista M. A., Mendoza C., Krolik J. H., 2004, ApJS, 155, 675
Kaspi S., Smith P. S., Netzer H., Maoz D., Jannuzi B. T., Giveon U., 2000, ApJ, 533, 631
Kim M., Peng C. Y., Barth A. J., Im M., Mertini P., Nelson C. H., 2008, ApJ, 688, 159
King A. R., 2003, ApJ, 596, L27
King A. R., Pounds K. A., 2003, MNRAS, 345, 657 (K03)
Marziani P., Sulentic J. W., Dultzin-Hacyan D., Clavani M., Moles M., 1996, ApJS, 104, 37
Murphy E. M., Lockman F. J., Laor A., Elvis M., 1996, ApJS, 105, 369
Pounds K. A., Page K. L., 2006, MNRAS, 372, 1275
Pounds K. A., Reeves J. N., 2007, MNRAS, 374, 823 (P07)
Pounds K. A., Reeves J. N., King A. R., Page K. L., O'Brien P. T., Turner M. J. L., 2003, MNRAS, 345, 705
Reeves J. N. et al., 2008, MNRAS, 385, 108
Risaliti G., Bianchi S., Matt G., Baldi A., Elvis M., Fabiano F., Zezas A., 2005, ApJ, 630, L129
Sobolewska M. A., Done C., 2007, MNRAS, 374, 150
Strüder L. et al., 2001, A&A, 365, L18
Tremaine S. et al., 2002, ApJ, 574, 740
Turner M. J. L. et al., 2001, A&A, 365, L27

APPENDIX A

Implicit in using the stacked spectral data to determine the energy, width and strength of the emission and absorption components of the Fe K profile is an assumption that the derived parameters are a true representation of the time-averaged values. In particular, it is important to confirm that the broad ionized emission line is not an artefact of the stacking procedure.

The ratio of each pn data set individually modelled to an absorbed power law in the energy band 3–10 keV is shown Fig. A1. Absorption and emission lines were then added to each data set, with line energy, width and flux free, and a new best fit obtained in each case. Table A1 shows the results. Although some individual parameters are not well constrained, and the absorption line is not formally detected in observation 2, the results are consistent with

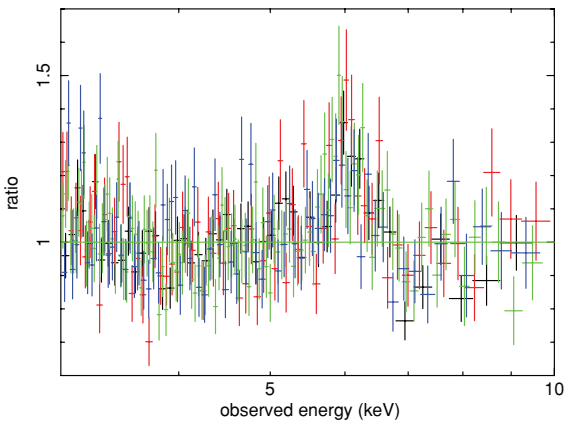

Figure A1. Fe K profiles for the individual pn data sets from the 2001 (black), 2004 (red), 2007a (green) and 2007b (blue) *XMM–Newton* observations of PG1211+143. The variable data quality reflects the effective exposures, which for the pn camera were 49, 33, 44 and 26 ks, respectively.

Table A1. Parameters of Gaussian absorption and emission lines fitted to the individual data sets displayed in Fig. A1.

Fit	Absorption line energy	Width	EW	Emission line energy	Width	EW	$\Delta\chi^2$/d.o.f.
Obs 1	7.62 ± 0.05	0.06 ± 0.03	-95 ± 30	6.63 ± 0.08	0.33 ± 0.10	135 ± 45	48/6
Obs 2	–	–	–	6.59 ± 0.07	0.25 ± 0.07	95 ± 45	24/6
Obs 3	7.59 ± 0.07	0.10 ± 0.06	-130 ± 45	6.58 ± 0.08	0.38 ± 0.08	160 ± 65	47/6
Obs 4	7.51 ± 0.15	0.25 ± 0.15	-100 ± 80	6.45 ± 0.17	0.46 ± 0.36	110 ± 65	14/6

Note. Line energies (adjusted to the AGN redshift) and 1σ line widths are in keV and EWs are in eV. The final column gives the improvement in χ^2 compared with the best-fitting absorbed power law over the 3–9 keV band.

those from the stacked data. A broad emission line is preferred in each individual data set.

For the RGS data, where we found evidence for a broad emission line of O VIII, the simultaneous detection of narrow lines of O VII provides direct support for the robustness of the stacking procedure. Again, as for the Fe XXV emission line, the large EW of the broad O VIII emission line is incompatible with a highly collimated outflow.

This paper has been typeset from a TEX/LATEX file prepared by the author.